

Titre: Modeling the thermal decomposition and residual mass of a carbon fiber epoxy matrix composite with a phenomenological approach: Effect of the reaction scheme
Title:

Auteurs: Jean Langot, Pablo Chávez-Gómez, Martin Lévesque, & Étienne Robert
Authors:

Date: 2022

Type: Article de revue / Article


Référence: Langot, J., Chávez-Gómez, P., Lévesque, M., & Robert, É. (2022). Modeling the thermal decomposition and residual mass of a carbon fiber epoxy matrix composite with a phenomenological approach: Effect of the reaction scheme. Fire and Materials, 46(1), 262-276. <https://doi.org/10.1002/fam.2974>
Citation:

 **Document en libre accès dans PolyPublie**
Open Access document in PolyPublie

URL de PolyPublie: <https://publications.polymtl.ca/10392/>
PolyPublie URL:

Version: Version finale avant publication / Accepted version
Révisé par les pairs / Refereed

Conditions d'utilisation: Tous droits réservés / All rights reserved
Terms of Use:

 **Document publié chez l'éditeur officiel**
Document issued by the official publisher

Titre de la revue: Fire and Materials (vol. 46, no. 1)
Journal Title:

Maison d'édition: Wiley
Publisher:

URL officiel: <https://doi.org/10.1002/fam.2974>
Official URL:

Mention légale: This is the peer reviewed version of the following article: Langot, J., Chávez-Gómez, P., Lévesque, M., & Robert, É. (2022). Modeling the thermal decomposition and residual mass of a carbon fiber epoxy matrix composite with a phenomenological approach: Effect of the reaction scheme. Fire and Materials, 46(1), 262-276. <https://doi.org/10.1002/fam.2974>, which has been published in final form at <https://doi.org/10.1002/fam.2974>. This article may be used for non-commercial purposes in accordance with Wiley Terms and Conditions for Use of Self-Archived Versions. This article may not be enhanced, enriched or otherwise transformed into a derivative work, without express permission from Wiley or by statutory rights under applicable legislation. Copyright notices must not be removed, obscured or modified. The article must be linked to Wiley's version of record on Wiley Online Library and any embedding, framing or otherwise making available the article or pages thereof by third parties from platforms, services and websites other than Wiley Online Library must be
Legal notice:



prohibited.

Modeling the thermal decomposition and residual mass of a carbon fiber epoxy matrix composite with a phenomenological approach: effect of the reaction scheme

Jean Langot^{a,*}, Pablo Chávez-Gómez^a, Martin Lévesque^a, Etienne Robert^a

^a*Polytechnique Montréal (2500 Chemin de Polytechnique, Montréal, QC H3T 1J4, Canada)*

Abstract

The thermal decomposition of Polymer Matrix Composites (PMCs) is a complex process involving hundreds of reactions and species which is often modeled with simplified one-step schemes. These schemes can be improved by adding intermediate reactions of different nature (competitive, parallel, consecutive). However, the optimal number and nature of intermediate reactions is rarely discussed. In this paper, several reaction schemes of increasing complexity have been developed to model the decomposition of a carbon/epoxy composite. The kinetic parameters describing each reaction have been extracted from Thermogravimetric Analysis (TGA) by means of isoconversional methods. The composite mass loss rate and residual mass have been modeled and compared to TGA and tube furnace data. This research shows that adding parallel or consecutive intermediate reactions improves the agreement against TGA data compared to a single-step model, but only competitive reactions can account for the variation of the residual mass observed in the tube furnace when the heating rate is varied.

Keywords: isoconversional methods, pyrolysis, oxidation, reaction mechanism, carbon/epoxy laminate, Polymer Matrix Composite, Thermogravimetric Analysis

*Corresponding author:

Email address: jean.langot@polymtl.ca (Jean Langot)

1. Introduction

Polymer Matrix Composites (PMCs), and more specifically carbon/epoxy composites, are extensively used in modern aircrafts [1], from cabin to primary and secondary structures, including the engines' "cold zone". For this test application, some powerplant components need to act as firewalls and must meet strict certification guidelines to ensure airworthiness [2]. Composites used in this context undergo thermal degradation, a complex phenomenon driven by several closely coupled thermal, chemical and physical processes [3]. Comprehensive pyrolysis models [4–7] have been developed to improve the understanding of composite degradation at high temperatures and support the design of new fire-resistant materials. These models are more versatile than empirical approaches, insofar as they are based on the conservation of mass, energy and momentum. However, comprehensive pyrolysis models require extensive material characterization, to estimate input parameters for the material properties as well as for the chemical reactions leading to the material decomposition.

Inaccuracies on input parameters can drastically reduce the model agreement against experimental data. However, sensitivity analyses have shown that the reaction scheme itself used to model the composite chemical decomposition has the most significant influence on its overall thermal behavior and more specifically on the material ignition, which leads rapidly to the complete degradation of the samples [8, 9]. In particular, the four parameters having the most influence on the average mass loss rate of a polymer exposed to a heat source are the activation energy, the pre-exponential factor, the heat of reaction and the char yield. Unfortunately, detailed reaction schemes are not available, as the thermal decomposition of a carbon/epoxy composites involves hundreds of reactions and intermediate species [10], that will vary with the composites chemical composition. This difficulty is compounded when considering the thermal decomposition of resins which constituents can change significantly between manufacturers. The lack of knowledge of the exact resin composition imposes the use of phenomenological approaches, based on mathematical interpretation of experimental

data taking into account the nature of the phenomena at play rather than strictly chemical and physical considerations. There is therefore a need to identify the appropriate level of complexity to implement in thermochemical decomposition models to improve their accuracy, taking into account the material properties that can conveniently be obtained experimentally for model inputs.

The complete reaction scheme is often summarized into one or a few global one-step reactions, in which the polymeric matrix decomposes into char and gas through pyrolysis [11–17]. This reaction can then be characterized with Thermogravimetric Analysis (TGA) or Differential Scanning Calorimetry (DSC) under an inert atmosphere using so-called isoconversional methods [18]. Several authors [19–22] improved their reaction scheme by adding intermediate reactions even if the real detailed mechanism remains partially, or totally, unknown. The intermediate reactions can either be competitive, parallel or consecutive [23]. For instance, Rein *et al.* [19] developed a five-step scheme composed of a combination of competitive and consecutive reactions to model the smoldering combustion of polyurethane foam. Lautenberger and Fernandez-Pello [24] modeled the oxidative pyrolysis of wood with a scheme composed of 4 consecutive heterogeneous reactions and 2 homogeneous reactions. Kim *et al.* [20] evaluated several reaction schemes describing the decomposition of fiberglass composites and concluded that increasing the complexity of the reaction scheme is sometimes unjustified. There is therefore a need to assess the ideal mechanism complexity as a function of the composite constituents.

For carbon/epoxy composites, McKinnon *et al.* [21] modeled the thermo-chemical decomposition of a laminate using TGA data, with consecutive reactions used to fit the complex shape of the single peak visible in the mass loss rate curve. Tranchard *et al.* [22] modeled the pyrolysis of an epoxy-based system with two main competitive reactions, to account for the variable residual mass observed when the heating rate is changed. In the aforementioned schemes, the knowledge of the chemical processes at play is only partial, which justifies the use of phenomenological approaches based on easily accessible experimental data. However,

in most cases, the influence of the nature and number of the reactions used has not been discussed. The existence of two fundamentally different schemes describing the thermo-chemical decomposition of the same type of matrix (i.e. epoxy resins) demonstrates that there is a need to systematically compare different phenomenological modeling approaches.

Moukhina [23] recently showed that several different reduced reaction schemes can capture the mass loss curve with a good agreement at specific heating rates, even if they are very different from the complete reaction scheme. The same author however pointed out that differences between models could increase when the heating rate is varied, in particular for the residual mass after thermal decomposition. This parameter depends directly on the char yield, which is very important in fire test simulation as it directly influences the quantity of insulating char formed on the hot face of the sample, protecting the composite from further heat transfer. The char yield also directly controls the proportion of combustible pyrolysates emitted to the surface and potentially leading to composite ignition, and is therefore a key parameter to predict the material mass loss rate in fire test [8]. Considering the difference of heating rates encountered in TGA ($1 - 50 \text{ K min}^{-1}$) and in a real fire test ($> 500 \text{ K min}^{-1}$), there is a need to optimize the reaction scheme not only in terms of mass loss rate but also residual mass. Unfortunately, the residual mass of a composite sample is subject to high variability in TGA because of the small size of the samples that cannot ensure a consistent matrix volume fraction in each sample, representative of the actual material composition. The volume fraction of each phase varies indeed locally in a composite [25, 26]. The use of an equipment able to degrade bigger samples, such as a tube furnace, can overcome this difficulty. In the literature, tube furnaces and TGA have already been used in combination to investigate plastic pyrolysis [27] or coal combustion [28].

The objective of this work is to investigate the influence of the nature and number of intermediate reactions on the ability of phenomenological thermal decomposition models to capture the mass loss rate and residual mass of PMCs. First, the theory of reaction rates in solids and isoconversional methods is reviewed and theoretical expressions for schemes

involving a variable number of intermediate reactions of different nature are derived. Then, kinetic parameters are obtained from TGA measurements with the isoconversional methods and used to develop schemes of increasing complexity. Finally, the choice of the nature and number of intermediate reactions in the reaction scheme is discussed by comparing the model outcomes to TGA and residual mass data. A carbon/epoxy material system is taken as an example in this study, but the method developed here is intended to be generalized on a wide variety of polymer composites evaluated in fire tests.

2. Theory

2.1. Background on reaction rate in solids

The decomposition rate of a solid exposed to a heat source is often represented by the degree of decomposition α , which is a parameter varying from 0 (material not degraded) to 1 (fully degraded material) as:

$$\alpha = \frac{m(t) - m_0}{m_\infty - m_0} \quad (1)$$

where $m(t)$, m_0 , m_∞ are the current, initial and final mass of the sample (kg). The reaction rate in solids can be calculated as a function of the temperature T (K), decomposition degree α and pressure P (Pa) as [18]:

$$\frac{d\alpha}{dt} = k(T)f(\alpha)h(P) \quad (2)$$

with $k(T)$ (s^{-1}) being the temperature-dependent decomposition rate. Assuming that the gaseous products are continuously evacuated, the pressure dependence can be neglected and $h(P) = 1$. The influence of the decomposition degree is accounted for by the reaction model $f(\alpha)$, which can take many different forms, whether the reaction is accelerating, decelerating or sigmoidal [18]. The most common reaction model is the n -order law $f(\alpha) = (1 - \alpha)^n$, where n is the reaction order ($-$). Finally, the temperature dependence is represented by

the Arrhenius equation:

$$k(T) = A \exp \left(-\frac{E}{RT} \right) \quad (3)$$

where A is the pre-exponential factor (s^{-1}), E the activation energy (J mol^{-1}) and R the ideal gas constant ($\text{J K}^{-1} \text{mol}^{-1}$). Combining Eqs. 2 and 3 provides the equation commonly used in kinetic analysis of solids exposed to heat as:

$$\frac{d\alpha}{dt} = \beta \frac{d\alpha}{dT} = f(\alpha) A \exp \left(-\frac{E}{RT} \right) \quad (4)$$

where β is the heating rate (K s^{-1}) obtained by the chain rule. The accuracy of the reaction scheme depends strongly on the kinetic triplet (A, E, n) that must be inferred experimentally, typically through Thermogravimetric Analysis (TGA) or Differential Scanning Calorimetry (DSC).

2.2. Background on isoconversional methods

The isoconversional principle states that the reaction rate at a constant extent of conversion is only a function of temperature, allowing the determination of the activation energy independently of the reaction model $f(\alpha)$. Isoconversional methods are divided in two categories: differential and integral methods, whether the analysis is performed on differential (DSC) or integral (TGA) data [18].

The differential isoconversional methods consist in taking the logarithm of Equation 4:

$$\ln \left(\beta \frac{d\alpha}{dT} \right)_{\alpha, \beta} = \ln(f(\alpha) A_{\alpha}) - \frac{E_{\alpha}}{RT_{\alpha}} \quad (5)$$

where the indices (α, β) denote respectively the specific decomposition degree and the heating rate at which the calculation is done. Then, assuming that $f(\alpha)$ is constant for each decomposition degree, the slope of the curve of $\ln \left(\beta \frac{d\alpha}{dT} \right)_{\alpha, \beta}$ plotted against $\frac{1}{T_{\alpha}}$ provides $-\frac{E_{\alpha}}{R}$. This method advantageously avoids the use of mathematical approximations or assumptions about the form taken by $f(\alpha)$, but the application of the differential method to integral data

requires numerical differentiation that induces noise, leading to inaccuracies [18].

The integral isoconversional methods are based on the direct analysis of integral data such as those provided by TGA. The integration of Equation 4 yields:

$$\int_0^\alpha \frac{d\alpha}{f(\alpha)} = \frac{A}{\beta} \int_0^T \exp\left(-\frac{E}{RT}\right) dT \quad (6)$$

Introducing the change of variable: $T = \frac{E}{Ry} \Rightarrow dT = -\frac{E}{Ry^2} dy$ leads to:

$$\int_0^\alpha \frac{d\alpha}{f(\alpha)} = -\frac{EA}{R\beta} \int_{+\infty}^{\frac{E}{RT}} \frac{\exp(-y)}{y^2} dy \quad (7)$$

The integral $p(y_f) = \int_{y_f}^\infty \frac{\exp(-y)}{y^2} dy$ (with $y_f = E/RT$) can be approximated by several methods after an integration by parts [29]. Starink [30] demonstrated that all mathematical approximations of Equation 7 can be summarized by the following general equation:

$$\ln\left(\frac{\beta}{T_\alpha^{k_1}}\right) = -k_2 \frac{E}{RT_\alpha} + k_3 \quad (8)$$

where the constants k_1 and k_2 depend on the integral approximation used. For instance, $(k_1; k_2) = (2; 1)$ in [31], $(k_1; k_2) = (0; 1.052)$ in [32, 33], $(k_1; k_2) = (1; 1)$ in [34] and $(k_1; k_2) = (1.92; 1.0008)$ in [30]. Flynn [35] insisted on the necessity to use an adequate approximation for the range considered for y_f . These approximations lose accuracy if y_f is small, typically $y_f < 15$ [30]. For epoxy pyrolysis, previous studies reported an activation energy close to 180 kJ mol⁻¹ [11, 36], which yields an y_f varying from 18 to 70. For this range, the Starink parameters offer the best accuracy and are thus used in this study. Depending on the values taken by the parameters E and A , several reaction models $f(\alpha)$ can describe a single experimental curve in cases of complex decomposition, where a linear relation exists between the apparent values of E and A [37]:

$$\ln(A_{\alpha,j}) = \frac{E_{\alpha,j}}{RT} + \ln\left[\frac{\beta d\alpha/dT}{f(\alpha)}\right]_{\alpha,j} = a_\beta + b_\beta E_{\alpha,j} \quad (9)$$

with $A_{\alpha,j}$ and $E_{\alpha,j}$ being the apparent Arrhenius parameters for each j reaction model and a_β and b_β constants depending on the heating rate β . In other words, Equation 9 states that a linear relation exists between $A_{\alpha,j}$ and $E_{\alpha,j}$, represented by so-called compensation lines of slope b_β in a semi-log of $\ln(A_{\alpha,j})$ as a function of $E_{\alpha,j}$. Once E_α has been determined by isoconversional methods, the corresponding value of A_α can be computed with this compensation principle. If the decomposition is described by a single-step reaction scheme, all the compensation lines intersect at the exact value of E and A . It is worth noting that this compensation approach is valid regardless of the reaction model that has been used to establish the linear relationship between E and A .

Then, the reaction model $f(\alpha)$ can be obtained by substituting different forms of $f(\alpha)$ into Equation 6 and comparing the curves obtained to experimental results.

Another method consists in assuming a general form for the reaction model, for instance $f(\alpha) = (1 - \alpha)^n$, and then finding n by mathematical optimization with a least-square algorithm. In that case, the square of the difference between measured and calculated data is minimized simultaneously for all the heating rates for which experimental data is available and for different values of n , until an optimal value is found providing the smallest residual [18]:

$$\text{Residue} = \sum_{i=1}^M [(x_{exp,i} - x_{num,i})^2] \quad (10)$$

where M is the number of different heating rates and x the variable on which the optimization is carried out, for instance α , or more frequently $d\alpha/dT$, owing to the high variations of this variable with time. This method provides a good quality of fit when optimizing smooth and regular peaks, but is less advantageous for irregular curves resulting from the overlapping of several peaks taking their origin in distinct chemical reactions. Numerical optimization can also be used to improve the values of E and A to be in better agreement with experimental data, starting from the values obtained by isoconversional methods as initial guesses.

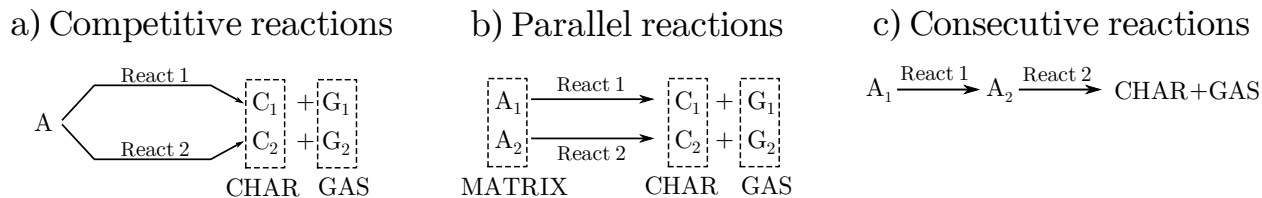


Figure 1: Examples of how two reactions can be arranged to form a simple reaction scheme involving a) competitive, b) parallel or c) consecutive reactions.

2.3. Development of multi-step schemes

It is generally admitted that the material decomposition can be modeled by a one-step scheme if the activation energy E_α , computed by means of isoconversional methods, varies by less than 10% with respect to the decomposition degree. However, a strong variation of E_α with respect to α reveals the presence of multi-step decomposition kinetics involving several reactions [23]. If several peaks are visible on the mass loss rate curve over temperature, they can be analyzed separately assuming that one peak represents one reaction. However, this is not always the case and several reactions can be overlapped into a single peak, making the analysis even more challenging. In that case, it can be difficult to determine if the reaction scheme is composed of competitive, consecutive, or parallel reactions (several schemes are represented on Figure 1 as an example), without prior knowledge of the complete chemical scheme which is in general unknown. Two very different schemes can model an experimental mass loss curve with a very good agreement at some heating rates, but differ when the heating rate is varied, which influences the residual mass after thermal decomposition [23]. For this reason, it is desirable to test different schemes involving a variable number of reactions of different nature, and observe the impact on the predicted residual mass.

A systematic equation accounting for a variable number of reactions can help tackle this difficulty. Equation 4 can be modified to account for multi-step reactions, provided that $f(\alpha)$ is known. However, as the number of reactions used to describe the composite decomposition is increased to consider multi-steps reaction schemes, it would be very difficult to use a different reaction model for each of these reactions. For this reason, the reaction model is assumed to follow a n -order law in this study.

Multi-steps schemes have already been derived for parallel reactions [18, 37], but as the equations developed in these works do not involve the char yield they therefore cannot be used to determine the residual mass after decomposition. Different equations describing the reaction rate of multiple reactions have been developed here, based on the variation of density instead of the decomposition degree in order to explicitly obtain the char yield θ_i . It is worth noting that in our approach the sample volume is assumed to remain constant. Equation 1 and 4 can be combined to compute the density variation of a species i associated with a single reaction j , assuming that each phase degrades completely (therefore $\bar{\rho}_{i,\infty} = 0$) as:

$$\left. \frac{d\bar{\rho}_i(t)}{dt} \right|_j = -\bar{\rho}_{i,0} \left[\frac{\bar{\rho}_i(t)}{\bar{\rho}_{i,0}(t)} \right]^{n_j} A_j \exp \left(-\frac{E_j}{RT} \right) \quad (11)$$

where ρ_i represents the density of species i (kg m^{-3}). The bar above the density indicates that the quantity is defined as a spatial average over the control volume. The total density change for a variable number of competitive, parallel and consecutive reactions can then be calculated with different methods, depending on the nature of the reaction scheme.

In the following, several theoretical formulations describing the density variation of a matrix decomposing with competitive, consecutive and parallel reactions are derived on an arbitrary control volume. The equations are first developed for a simple case involving only two reactions, as represented on Figure 1, and are then generalized to N equations.

2.3.1. Competitive reactions

A solid phase is composed of a single species A that can be decomposed following exposure to heat into species C_1 and C_2 , both representative of the char, through two independent competitive reactions, as shown schematically in Figure 1a). The total density is given by:

$$\rho_{tot} = \bar{\rho}_A + \bar{\rho}_{C1} + \bar{\rho}_{C2} \quad (12)$$

which leads to:

$$\frac{d\rho_{tot}}{dt} = \frac{d\bar{\rho}_A}{dt} + \frac{d\bar{\rho}_{C1}}{dt} + \frac{d\bar{\rho}_{C2}}{dt} \quad (13)$$

Substituting Equation 11 into Equation 13 yields:

$$\begin{aligned}
\frac{d\rho_{tot}}{dt} &= -\bar{\rho}_{A,0} \left(\frac{\bar{\rho}_A}{\bar{\rho}_{A,0}} \right)^{n_1} k_1(T) + \theta_1 \bar{\rho}_{A,0} \left(\frac{\bar{\rho}_A}{\bar{\rho}_{A,0}} \right)^{n_1} k_1(T) \\
&\quad - \bar{\rho}_{A,0} \left(\frac{\bar{\rho}_A}{\bar{\rho}_{A,0}} \right)^{n_2} k_2(T) + \theta_2 \bar{\rho}_{A,0} \left(\frac{\bar{\rho}_A}{\bar{\rho}_{A,0}} \right)^{n_2} k_2(T) \\
&= \bar{\rho}_{A,0} \left[(\theta_1 - 1) \left(\frac{\bar{\rho}_A}{\bar{\rho}_{A,0}} \right)^{n_1} k_1(T) + (\theta_2 - 1) \left(\frac{\bar{\rho}_A}{\bar{\rho}_{A,0}} \right)^{n_2} k_2(T) \right]
\end{aligned} \tag{14}$$

Equation 14 can be generalized to N reactions as:

$$\frac{d\rho_{tot}}{dt} = \bar{\rho}_{A,0} \sum_{i=1}^N (\theta_i - 1) \left[\left(\frac{\bar{\rho}_A}{\bar{\rho}_{A,0}} \right)^{n_i} k_i(T) \right] \tag{15}$$

2.3.2. Parallel reactions

A solid phase is composed of two species A_1 and A_2 , with a volume fraction of respectively $X_{A,1}$ and $X_{A,2}$. When the material is exposed to heat, A_1 and A_2 decomposes into species C_1 and C_2 through two independent parallel reactions, as represented in Figure 1b). The total density is given by:

$$\begin{aligned}
\rho_{tot} &= X_{A1}(\rho_{A1} + \rho_{C1}) + X_{A2}(\rho_{A2} + \rho_{C2}) \\
&= (\bar{\rho}_{A1} + \bar{\rho}_{C1}) + (\bar{\rho}_{A2} + \bar{\rho}_{C2})
\end{aligned} \tag{16}$$

Equation 16 can be differentiated with respect to time to obtain the mass loss rate as:

$$\frac{d\rho_{tot}}{dt} = \left(\frac{d\bar{\rho}_{A1}}{dt} + \frac{d\bar{\rho}_{C1}}{dt} \right) + \left(\frac{d\bar{\rho}_{A2}}{dt} + \frac{d\bar{\rho}_{C2}}{dt} \right) \tag{17}$$

Substituting Equation 11 into Equation 17 yields:

$$\begin{aligned}
\frac{d\rho_{tot}}{dt} &= \left(-\bar{\rho}_{A1,0} \left(\frac{\bar{\rho}_{A1}}{\bar{\rho}_{A1,0}} \right)^{n_1} k_1(T) + \theta_1 \bar{\rho}_{A1,0} \left(\frac{\bar{\rho}_{A1}}{\bar{\rho}_{A1,0}} \right)^{n_1} k_1(T) \right) \\
&\quad + \left(-\bar{\rho}_{A2,0} \left(\frac{\bar{\rho}_{A2}}{\bar{\rho}_{A2,0}} \right)^{n_2} k_2(T) + \theta_2 \bar{\rho}_{A2,0} \left(\frac{\bar{\rho}_{A2}}{\bar{\rho}_{A2,0}} \right)^{n_2} k_2(T) \right) \\
&= (\theta_1 - 1) \left[\bar{\rho}_{A1,0} \left(\frac{\bar{\rho}_{A1}}{\bar{\rho}_{A1,0}} \right)^{n_1} k_1(T) \right] + (\theta_2 - 1) \left[\bar{\rho}_{A2,0} \left(\frac{\bar{\rho}_{A2}}{\bar{\rho}_{A2,0}} \right)^{n_2} k_2(T) \right] \quad (18)
\end{aligned}$$

Equation 18 can be generalized to N reactions as:

$$\frac{d\rho_{tot}}{dt} = \sum_{i=1}^N (\theta_i - 1) \left[\bar{\rho}_{i,0} \left(\frac{\bar{\rho}_i}{\bar{\rho}_{i,0}} \right)^{n_i} k_i(T) \right] \quad (19)$$

2.3.3. Consecutive reactions

Consider a solid phase composed of a single species A_1 . When the material is exposed to heat, A_1 decomposes into species A_2 , and then A_2 decomposes into C , as represented in Figure 1c). The total density is given by:

$$\rho_{tot} = \bar{\rho}_{A1} + \bar{\rho}_{A2} + \bar{\rho}_C \quad (20)$$

which leads to:

$$\frac{d\rho_{tot}}{dt} = \frac{d\bar{\rho}_{A1}}{dt} + \frac{d\bar{\rho}_{A2}}{dt} + \frac{d\bar{\rho}_C}{dt} \quad (21)$$

Substituting Equation 11 into Equation 21 yields:

$$\begin{aligned}
\frac{d\rho_{tot}}{dt} &= -\bar{\rho}_{A1,0} \left(\frac{\bar{\rho}_{A1}}{\bar{\rho}_{A1,0}} \right)^{n_1} k_1(T) + \theta_1 \bar{\rho}_{A1,0} \left(\frac{\bar{\rho}_{A1}}{\bar{\rho}_{A1,0}} \right)^{n_1} k_1(T) \\
&\quad - \bar{\rho}_{A2,0} \left(\frac{\bar{\rho}_{A2}}{\bar{\rho}_{A2,0}} \right)^{n_2} k_2(T) + \theta_2 \bar{\rho}_{A2,0} \left(\frac{\bar{\rho}_{A2}}{\bar{\rho}_{A2,0}} \right)^{n_2} k_2(T) \quad (22)
\end{aligned}$$

$\bar{\rho}_{A_2,0}$ represents the density of the intermediate specie A_2 with respect to the control volume, whose value is unknown. It is assumed in this work that $\bar{\rho}_{A_2,0}$ and $\bar{\rho}_{C,0}$ can be computed from the density of the initial species through the char yield θ : $\bar{\rho}_{A_2,0} = \theta_1 \bar{\rho}_{A_1,0}$ and $\bar{\rho}_{C,0} = \theta_2 \bar{\rho}_{A_2,0} = \theta_1 \theta_2 \bar{\rho}_{A_1,0}$. This assumption yields:

$$\frac{d\rho_{tot}}{dt} = \bar{\rho}_{A_1,0} \left[(\theta_1 - 1) \left(\frac{\bar{\rho}_{A_1}}{\bar{\rho}_{A_1,0}} \right)^{n_1} k_1(T) + \theta_1(\theta_2 - 1) \left(\frac{\bar{\rho}_{A_2}}{\theta_1 \bar{\rho}_{A_1,0}} \right)^{n_2} k_2(T) \right] \quad (23)$$

Equation 23 can be generalized to N reactions as:

$$\frac{d\rho_{tot}}{dt} = \bar{\rho}_{A_1,0} \left[\sum_{i=1}^N \gamma_i (\theta_i - 1) \left(\frac{\bar{\rho}_i}{\gamma_i \bar{\rho}_{A_1,0}} \right)^{n_i} k_i(T) \right] \quad (24)$$

with $\gamma_i = 1$ if $i = 1$ and $\gamma_i = \prod_{j=1}^{i-1} \theta_j$ the rest of time.

3. Experimental methods

3.1. Materials

The material studied is a 1.6 mm-thick, quasi-isotropic laminate fabricated from an aerospace-grade carbon/epoxy pre-preg system (reinforcement: woven carbon fiber HTS40 E13 3K PW), procured from Solvay (formerly CYTEC, Tulsa, OK). Samples for TGA and tube furnace tests were extracted therefrom considering its full thickness. The matrix represents 41.76% of the total weight. The exact composition of the epoxy resin system is a trade secret and, therefore, could not be obtained from the manufacturer, which forces the use of phenomenological approaches to characterize its decomposition.

3.2. Thermogravimetric Analysis & Differential Scanning Calorimetry

Simultaneous Differential Scanning Calorimetry (DSC) and TGA measurements have been performed using a TGA/DSC 1 apparatus (Mettler-Toledo, Columbus, OH) in both inert (N_2 , 60 ml min⁻¹) and oxidative (air, 60 ml min⁻¹) environments, under atmospheric pressure. The samples were placed in 70 μ l open alumina crucibles and exposed to three

| Apparatus | Heating rate (K min ⁻¹) | Sample mass (mg) | | | |
|--------------|-------------------------------------|------------------|-------|---------|-------|
| STA | | N ₂ | | Air | |
| | 5 | 10.6980 | | 10.3630 | |
| | 10 | 14.9319 | | 15.2581 | |
| | 25 | 12.0205 | | 11.0230 | |
| Tube furnace | | N ₂ | | | |
| | 1 | 899.7 | 893.9 | 780.0 | 792.3 |
| | 3 | 768.6 | 768.0 | 901.0 | 782.0 |
| | 5 | 539.2 | 563.4 | 555.1 | 557.4 |

Table 1: Heating rates and mass of the samples used in STA and tube furnace runs.

different heating rates of 5, 10 and 25 K min⁻¹, as platinum may act as a catalyst on the oxidation of carbon fibers [38]. The heating rates and the corresponding sample mass are reported in Table 1.

3.3. Tube furnace

The residual mass relative to the initial value of a composite sample is difficult to assess using TGA, from the high variability between runs, as the small size of the sample does not ensure a consistent volume fraction for each constituent of the composite [39, 40]. For this reason, a tube furnace (Carbolite Gero STF furnace tube) was selected as a complementary approach to TGA to estimate the composite residual mass after decomposition, to overcome the limitations of the finite sample size. This instrument allows the pyrolysis of samples an order of magnitude heavier (500 – 900 mg) than those used in TGA (10 – 20 mg), while placed in an open alumina pan. The three sets of 4 samples were heated at different rates until reaching 1000 °C, then kept at constant temperature for one hour, before letting the sample cool naturally. The maximum heating rate is however much lower than in a TGA, limited to 5 K min⁻¹ by the capability of the equipment. Once the samples reach room temperature, they were weighed with a high precision scale (10⁻⁴ g). Inert environment was ensured by a constant Argon flow (1317 ml min⁻¹). No residue is observed in the pan at the end of the experiment, suggesting that the inert flow is high enough to efficiently evacuate the gasses emitted by chemical reactions.

4. Results and Discussions

4.1. Experimental results

4.1.1. TGA / DSC

Figure 2 shows the variation of the sample mass as a function of temperature for three different heating rates obtained from the TGA under inert (Figure 2a) and oxidative atmospheres (Figure 2d). The variation of the degree of decomposition $d\alpha/dT$ is also shown as a function of temperature under inert (Figure 2b) and oxidative atmospheres (Figure 2e). Figure 2c) represents the heat flow transmitted to the sample as a function of temperature under an inert atmosphere for a single heating rate (10 K min^{-1}), with the corresponding $d\alpha/dT$ curve. The hatched area corresponds to the heat absorbed or released by chemical reactions or physical changes occurring in the sample during its decomposition.

Under an inert atmosphere, the composite decomposition starts at 500 K and is complete above 900 K, accompanied by a mass loss of approximately 26.5%. This reaction is typically associated with pyrolysis as it does not require the presence of reactive species. The resin represents 41.76% of the total composite weight, with the remaining mass corresponding to the sum of the fibers, which are non-reactive under an inert atmosphere, and the residues (char) from resin decomposition. The variations in residual mass observed between runs in Figure 2a) are mostly the result of the small size of the samples used for TGA, that cannot ensure a composition representative of the actual composite. As a consequence, it is not possible to clearly identify a trend in the variations of residual mass (*i.e.* a monotonic variation). This justifies the use of bigger samples in a tube furnace to measure the residual mass. A single peak is visible on Figure 2b), shifting to the right as the heating rate is increased. This shifted single peak suggests that, under inert atmosphere, the phenomena at play can be captured by a single reaction. However, at least three reactions absorbing/releasing heat can be observed in the corresponding DSC data of Figure 2c). This demonstrates that several reactions are overlapped into the single TGA peak, highlighting the need to develop multi-steps reaction schemes. It must be emphasized that the measurements provided by

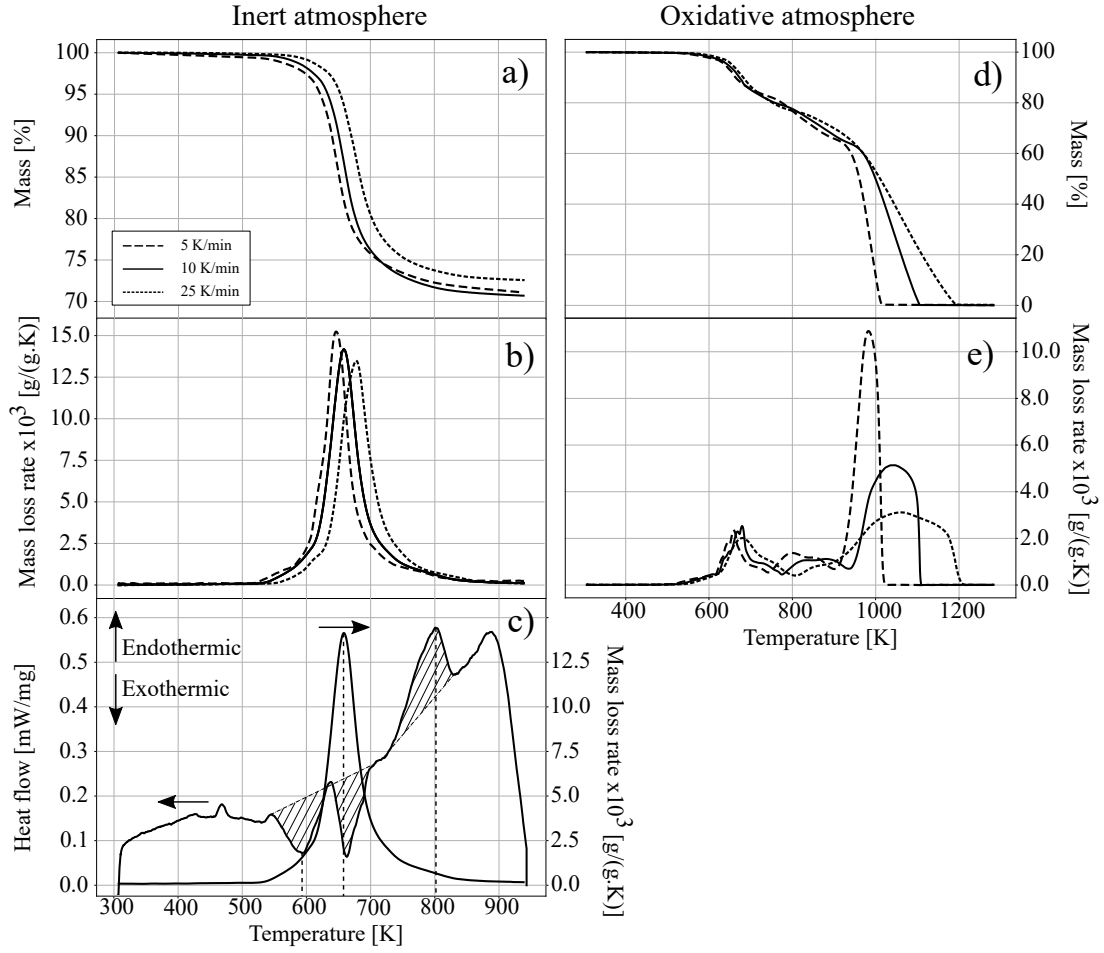


Figure 2: Variation of mass, mass loss rate and heat flow per unit mass as a function of temperature under inert a)-b)-c) and oxidative d)-e) atmospheres. The heating rate for c) is 10 K min^{-1} .

| Heating rate (K min ⁻¹) | Matrix pyrolysis (K) | | Char oxidation (K) | | Fiber oxidation (K) | |
|--|----------------------|------|--------------------|------|---------------------|------|
| | Range | Peak | Range | Peak | Range | Peak |
| 5 | 500 – 740 | 660 | 740 – 900 | 679 | 900 – 1013 | 681 |
| 10 | 500 – 773 | 800 | 773 – 935 | 840 | 935 – 1103 | 860 |
| 25 | 500 – 805 | 983 | 808 – 936 | 1045 | 936 – 1189 | 1061 |

Table 2: For each decomposition step isolated from the curves of Figure 2, temperature range over which they occur and temperature at the peak.

the DSC are qualitative and not quantitative, as the DSC was not calibrated to measure the heat of reaction.

Figure 2e) shows three different peaks in the TGA curves, hinting at the presence of at least three different reactions under an oxidative atmosphere. The first occurs between 500 and 800 K, and is associated with matrix pyrolysis. The two other peaks correspond to the char and fiber oxidation, which requires the presence of oxygen diffusing within the porous sample. The different peaks are very irregular, when compared to those obtained under an inert atmosphere, making data analysis challenging. The temperature ranges of each peak are reported in Table 2.

4.1.2. Tube furnace

Figure 3 presents the residual mass means after treatment in the tube furnace for three different heating rates: 1, 3 and 5 K min⁻¹. The variation of residual mass observed in the tube furnace (72.5 and 74.6%) is quantitatively similar to the one observed in TGA (71 and 73%); however, contrary to the results obtained with TGA, the residual mass decreases monotonically with an increasing heating rate. This again reveals that several reactions are at play, as a single decomposition step is associated to a unique char yield and therefore cannot provide different residual masses when the heating rate is changed. Therefore, the Tube Furnace provides useful information about the actual reaction mechanism. The variation of residual mass remains quantitatively low, but could increase at higher heating rates. Moreover, the variation of residual mass is given for the entire composite, which contains 41.76% of matrix in mass and 58.24% of fibers (non-reactive under inert atmosphere). Therefore, the variation of residual mass is much more important with respect to the matrix only.

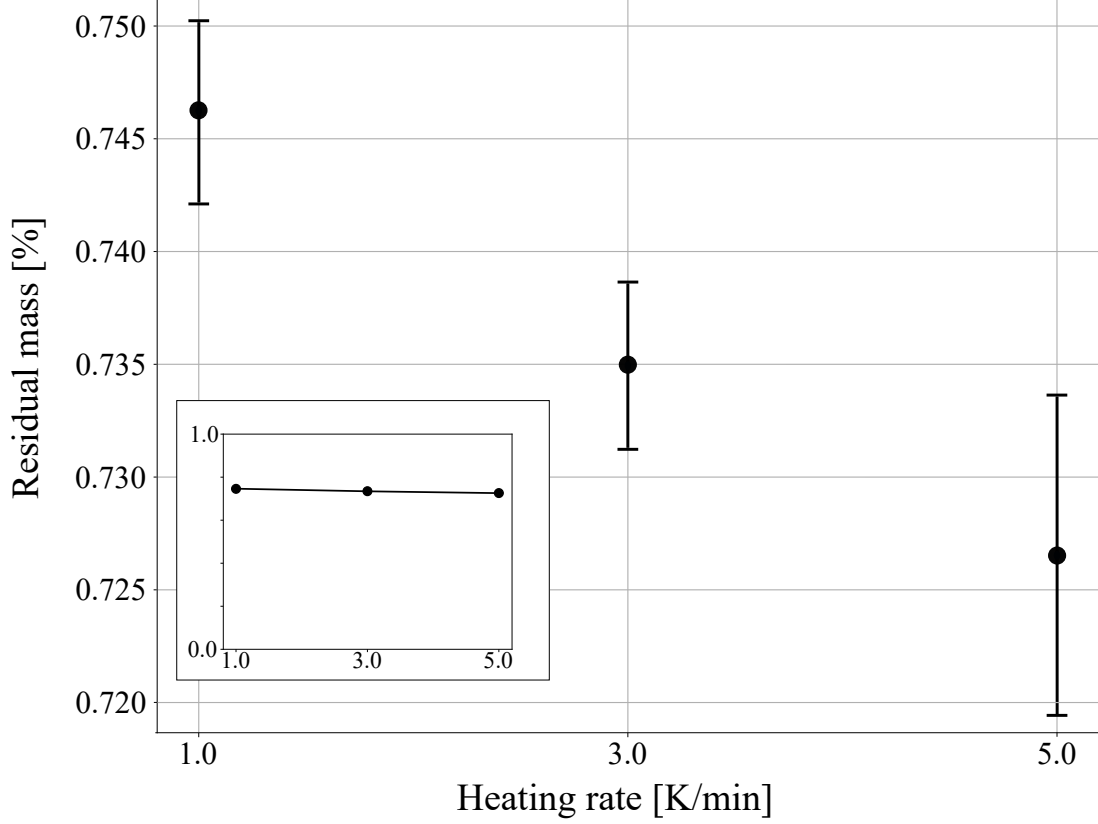


Figure 3: Residual mass means obtained after decomposition in a tube furnace at three different heating rates: 1, 3 and 5 K min⁻¹. Error bars show the 95% confidence intervals considering Student's t distribution.

The error bars on Figure 3 show the 95% confidence intervals (CI) using Student's t distribution, appropriate for small data sets. Data show limited error because of the important size of the samples that ensures a similar volume fraction of each constituent in all samples. The error increases slightly for $\beta = 5$ K min⁻¹, possibly because of the smaller sample size (see Table 1), or because of equipment limitations at higher heating rates. Upon visual examination, there is an overlap of CIs between data from 3 and 5 K min⁻¹; therefore, a t -test was performed ($t = 3.327$, $p = 0.0159$). Thus, the residual mass means of the aforementioned heating rates can be considered statistically different at a 95% CI. The low data error suggests that tube furnaces could be more appropriate than TGA to estimate the residual mass of a composite sample after thermal decomposition due to variation of matrix volume fraction which depending on the location of the sample extraction, as demonstrated for woven configurations [25].

4.2. Thermochemical parameters

Isoconversional methods have been used to infer the activation energy and pre-exponential factor from TGA measurements, following to the method described in Section 2.2. Figure 4a) reveals the evolution of the activation energy as a function of the decomposition degree, under an inert atmosphere. The activation energy increases rapidly from almost 0 at $\alpha = 0$ to 185 kJ mol^{-1} at $\alpha = 0.3$. A plateau is subsequently reached and the activation energy remains almost constant until $\alpha = 0.7$. This plateau most likely corresponds to the main pyrolysis step of epoxy decomposition. The activation energy at the plateau is in agreement with previous values reported in the literature for other types of epoxy resins [11–13, 15, 16]. The activation energy increases again above $\alpha = 0.7$, reaching a peak of $E = 447 \text{ kJ mol}^{-1}$ for $\alpha = 0.92$ and sharply decreasing thereafter. An activation energy increasing with decomposition degree is a typical behavior observed several times for epoxy matrices [11, 22]. Very reactive species, i.e. with low activation energies, react first whereas the less reactive species react only later as the temperature becomes sufficiently high. Only the very weakly reactive species remain at the end of the decomposition process, which explains the peak observed at $\alpha = 0.92$ on Figure 4a). The value reached at the peak and the decrease after $\alpha = 0.92$ have limited physical meaning and could be caused by a loss of validity of the isoconversional methods for high decomposition degree, *i.e.* above $\alpha = 0.9$. Nevertheless, the pyrolysis process can be modeled as a one-step reaction if the activation energy is almost constant (less than 10% of variation) over a wide range of decomposition degrees [41]. This is not the case here as strong variations of E can be observed for $\alpha \leq 0.3$ and $\alpha \geq 0.7$, further motivating the need of implementing more complex reaction schemes.

Figure 4b) represents the evolution of the pre-exponential factor as a function of the activation energy. The dots represent the different reaction models for which the couple (E, A) has been calculated. Four n -order reaction model have been evaluated with a reaction order n successively equal to 1, 2, 3, and 4. With this approach, it is generally admitted that if the thermo-chemical decomposition can be summarized as a single-step reaction, the compensa-

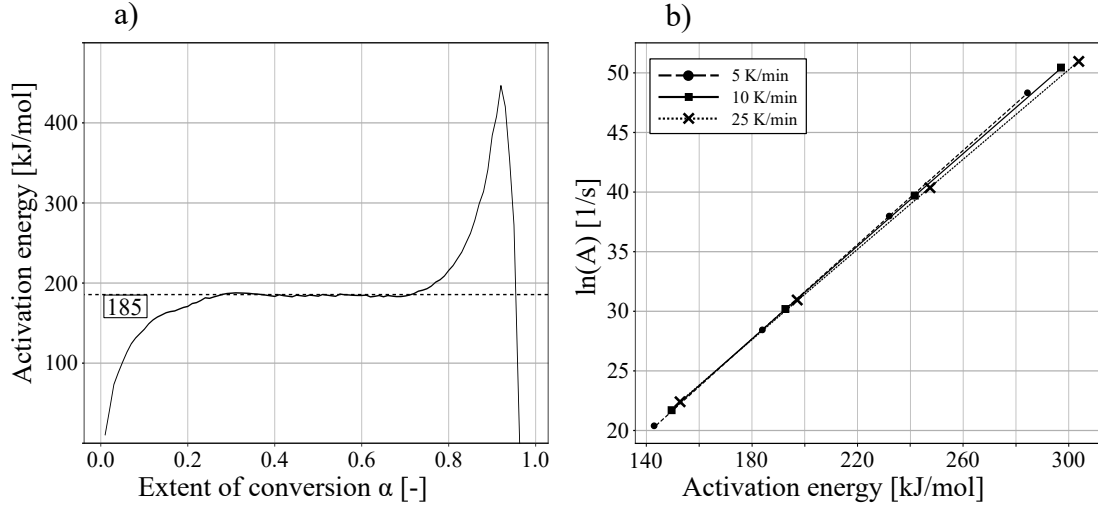


Figure 4: a) Evolution under inert atmosphere of the activation energy as a function of the extent of conversion, as evaluated using isoconversional methods and b) pre-exponential factor as a function of the activation energy, from the compensation principle.

tion lines cross each other at a single point, whose coordinates (E, A) provide the activation energy and pre-exponential factor of the reaction. Here, the compensation lines do not cross at a single point, which again motivates the need to develop multi-step reaction schemes.

As the decomposition is much more complicated under oxidative atmosphere, the activation energy has been computed independently for each of the three peaks observed on Figure 2e), according to the ranges reported in Table 2. Figure 5a), 5c) and 5e) show the evolution of the activation energy as a function of a normalized decomposition degree under an oxidative atmosphere, for each step (matrix pyrolysis, char oxidation, fiber oxidation). It can be observed that the activation energy of the matrix pyrolysis is significantly lower under an oxidative atmosphere than under an inert one. This phenomenon has already been observed for epoxy resins in previous studies [39, 42] and could be related to an early pre-oxidation of highly reactive epoxy resin components before the onset of pyrolysis [39, 43]. This could also be the result of the activation energy for the char oxidation at low conversion degree (112 kJ mol^{-1} on Figure 5) being lower than the activation energy of the matrix pyrolysis under inert atmosphere (185 kJ mol^{-1}). Consequently, the char can be oxidized as soon as it is formed, reducing the activation energy of the composite when considered as a whole,

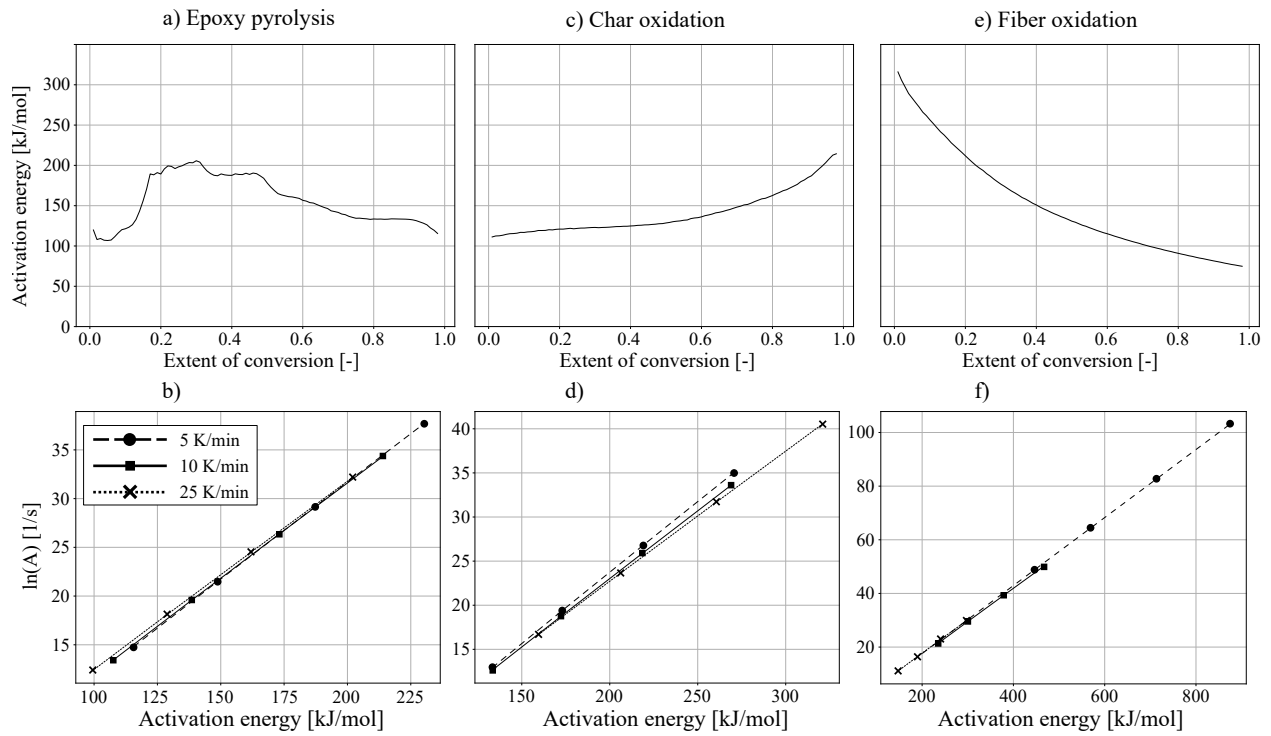


Figure 5: a), c), e): Evolution under oxidative atmosphere of the activation energy as a function of the extent of conversion for respectively epoxy pyrolysis, char oxidation and fiber oxidation. b), d), f): evolution of the pre-exponential factor as a function of the activation energy for respectively epoxy pyrolysis, char oxidation and fiber oxidation.

for low decomposition degrees. The pyrolysis activation energy reported on Figure 5a) could thus be a weighted mean of the activation energies related to matrix pyrolysis and early char oxidation. As the decomposition degree progresses, the activation energy for matrix pyrolysis under an oxidative atmosphere seems to reach a plateau of approximately 185 kJ mol^{-1} for $\alpha = 0.2$ but decreases after $\alpha = 0.5$, further supporting this hypothesis. However, it is difficult to reach a definitive conclusion because of the irregularity of the first and second peaks on Figure 2e), making the calculation of the activation energy inaccurate, particularly for char oxidation. Finally, Figure 5e) represents the activation energy for fiber oxidation. It starts at a high value ($E = 315 \text{ kJ mol}^{-1}$) and decreases regularly thereafter, until reaching 75 kJ mol^{-1} at the end of the decomposition. This behavior could be explained by the typical structure of PAN-based carbon fibers, which have a turbostratic/graphitic outer skin that protects the amorphous and more reactive core [44]. Another explanation is the heterogeneous nature of carbon-oxygen kinetics [45, 46]. Halbig *et al.* [46] performed TGA runs on T-300 carbon fibers at different temperatures and suggested the existence of two regimes: (i) a low temperature regime (720-1150K) associated with high activation energy, where oxidative species are in excess; (ii) a high temperature regime (870-1700K) associated with low activation energy, where the reaction rate is controlled by the diffusion of oxidative species. Each of these regimes could be modeled with a specific reaction model $f(\alpha)$. However, the two regimes are likely to coexist in our case because of the large temperature range encountered in both fire test and TGA. The decreasing of the activation energy of carbon fiber oxidation observed on Figure 5e) tends to confirm the existence of a transition between the two regimes. For this reason, a more versatile n -order reaction model will be used to develop an aerobic reaction scheme in Section 4.3.2, because of the lack of a reaction model describing simultaneously these two regimes.

Figure 5b), 5d) and 5f) represent the evolution of the pre-exponential factor as a function of the activation energy. For all reactions considered, it is difficult to define a particular point where the compensation lines cross, although for pyrolysis it appears to be positioned at

high values for the (E, A) pair. For both char and fiber oxidation, this crossing point is likely located near the lower bounds of the (E, A) range obtained.

4.3. Numerical results

4.3.1. Single-step schemes: anaerobic decomposition

Mathematical optimization was used to identify the order of reaction n as well as to optimize the activation energy E and the pre-exponential factor A . First, an average value E_{av} was computed from the values reported in Figure 4a). A corresponding pre-exponential factor A_{av} was calculated using the compensation parameters determined from Figure 4b). The data set (E_{av}, A_{av}) was used as an initial guess in the optimization process. E and A were optimized within a range centered on (E_{av}, A_{av}) : E was varied between $0.8E_{av}$ and $1.2E_{av}$, and A was varied between $10^{-3}A_{av}$ to 10^3A_{av} . The reaction order n was optimized between 1.0 and 5.0.

The residue (Equation 10) was computed using two different methods for the pyrolysis: with $x = \alpha$ and with $x = d\alpha/dT$, to compare both methods. The residue was minimized to find optimal values for (E, A, n) with the least-squared algorithm method, using the package "LMFIT" in Python [47]. In order to avoid misinterpreting a local minimum, the initial value E_{av} was varied to verify if the solution is valid regardless of the initial guess. Finally, once the complete kinetic triplet is identified, the char yield is calculated by minimizing the difference between numerical and experimental residual mass over all the heating rates used in the tube furnace, with the char yield θ varying from 0 to 1.

The single-step schemes accounting for matrix pyrolysis under an inert atmosphere are reported in Table 3. The coefficient of determination R^2 indicates the quality of fit between the experimental and numerical values of the quantity optimized (α or $d\alpha/dT$) for all the heating rates. The two schemes obtained by optimizing α and $d\alpha/dT$ are very similar; however, the optimization based on α provides a better coefficient of determination than that based on $d\alpha/dT$. There is no clear threshold of R^2 stating that a numerical reaction scheme can or cannot model the actual decomposition, but previous studies aimed at maximizing this coef-

| Reaction | Quantity minimized | E (kJ mol ⁻¹) | A (s ⁻¹) | n (-) | θ (-) | R^2 (-) |
|-----------|--------------------|-----------------------------|------------------------|---------|--------------|-----------|
| Pyrolysis | α | 193 | 2.20×10^{13} | 3.03 | 0.3678 | 0.9983 |
| | $d\alpha/dT$ | 199 | 5.26×10^{13} | 2.43 | 0.3678 | 0.9614 |

Table 3: Reaction scheme of a carbon fiber epoxy matrix composite exposed to an inert atmosphere for heating rates $\beta = 5, 10, 25$ K min⁻¹.

ficient to choose their reaction scheme. When modeling pyrolysis, R^2 typically ranges from 0.95 to 0.99 [17], and optimizing the reaction scheme with α instead of $d\alpha/dT$ improved the R^2 from 0.96 to 0.99. This reveals that the integral value is easier to fit than its derivative, probably due to the strong variations of $d\alpha/dT$ on Figure 2b). The value obtained for E is also slightly larger than the initial guess E_{av} for both schemes. The char yield θ calculated here corresponds to an averaged residual mass over the three heating rates used in the tube furnace, as it is impossible to obtain a residual mass that varies as a function of the heating rate with a single-step scheme. This shows that despite the good mathematical agreement obtained with TGA data, a single-step scheme cannot capture the variations of residual mass observed as a function of the heating rate and therefore misses some information inherent to the actual mechanism.

4.3.2. Multi-steps schemes: aerobic decomposition

From the experimental data collected for thermal decomposition under an oxidative atmosphere, the multi-step mechanism leading to the material aerobic decomposition has been modeled with three single step reactions, obtained from distinct peaks in the TGA data. From these single-step reactions, one can then build a multi-step scheme with 2 consecutive reactions and 1 parallel reaction, as shown schematically on Figure 6, to account for matrix pyrolysis, char oxidation and fiber oxidation. The method used to infer the kinetic triplet is similar to the one developed in Section 4.3: average values (E_{av} , A_{av}) are computed for each reaction on Figure 5 and are optimized in a narrowed range ($\pm 20\%$). The only difference being on the choice of the variable optimized with Equation 10: because of the irregularity of the mass loss rate peaks on Figure 2e), the residue was calculated solely with $x = \alpha$ for the reactions under an oxidative atmosphere.

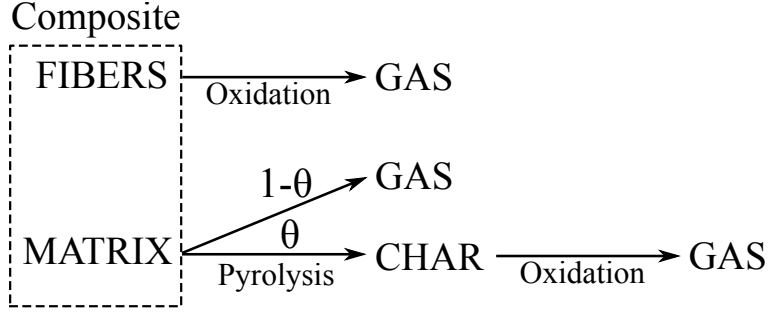


Figure 6: Reaction scheme describing the chemical decomposition of a carbon epoxy composite exposed to an oxidative atmosphere.

| Thermo-Oxidative Decomposition | Quantity minimized | E (kJ mol ⁻¹) | A (s ⁻¹) | n (-) | θ (-) | R^2 |
|--------------------------------|--------------------|-----------------------------|------------------------|---------|--------------|--------|
| Pyrolysis | α | 148 | 2.26×10^9 | 3.13 | 0.3678 | 0.9955 |
| Char oxidation | α | 112 | 1.70×10^4 | 1.76 | - | 0.9938 |
| Fiber oxidation | α | 260 | 4.93×10^{10} | 4.83 | - | 0.9907 |

Table 4: Scheme composed of single-step reactions of a carbon fiber epoxy matrix composite exposed to an oxidative atmosphere for heating rates $\beta = 5, 10, 25$ K min⁻¹.

The kinetic triplet for each reaction are reported in Table 4. Globally, the optimization confirmed the previous estimation of E and A obtained from isoconversional methods, except for the activation energy related to fiber oxidation which is more important than its average value on Figure 5c).

4.3.3. Multi-steps schemes: anaerobic decomposition

Section 4.3.1 revealed that a single-step reaction scheme can model the mass loss rate of the epoxy resin with a good agreement against TGA data, but is unable to capture the variation of residual mass observed in the tube furnace. For this reason, several reaction schemes specifically developed for epoxy pyrolysis are proposed in this section, including intermediate reactions of different nature: competitive, parallel or consecutive. The initial values of activation energy E_i are first distributed in the range observed on Figure 4, i being the reaction number. Then, the corresponding values of pre-exponential factor A_i are calculated with the compensation principle. Finally, the density variation is computed with Equations 15, 19, 24 and each set of parameters (E_i, A_i, n_i) is optimized simultaneously by minimizing the residue calculated using Equation 10. For instance, the initial activation energies of three-parallel intermediate reactions are $[E_1, E_2, E_3]=[80, 160, 220]$ kJ mol⁻¹, and then these values are

optimized in the range $[80 \pm 20\%, 160 \pm 20\%, 220 \pm 20\%]$. Therefore, the activation energies of the multi-steps schemes is distributed in the entire range observed on Figure 4a). Moreover, the initial values $[E_1, E_2, E_3]$ were varied to avoid misinterpreting local minimum. It is worth noting that the optimization is carried out in this section on $x = d\alpha/dT$ only, because the complex shape of $d\alpha/dT$ allows a more accurate optimization when several reactions are at play. E_i is varied between $0.8 \times E_i$ and $1.2 \times E_i$, A_i between $A_i \times 10^{-3}$ and $A_i \times 10^3$ and n_i between 0 to 5. If the scheme includes parallel reactions, another parameter X_i varying between 0 and 1 describing the volume fraction of the sub-phases composing the matrix is also optimized simultaneously, with the constraint $\sum_{i=1}^N X_i = 1$. Then, an optimal value of the char yield θ_i between 0 and 1 is obtained in a second step by minimizing the residue calculated using Equation 10 with x being the residual mass at the end of the test.

Figure 7 represents the quality of fit of the numerical mass loss rate $d\alpha/dT$ against TGA data for each scheme (competitive, parallel, consecutive). The x -axis is the number of reactions and the y -axis is the evolution of the coefficient of determination R^2 . Figure 8 shows a comparison between numerical and experimental mass loss rate for $\beta = 10 \text{ K min}^{-1}$ for four different reaction schemes: single-step, three competitive, three consecutive, three parallel. The scheme composed of parallel reactions offers the best agreement against experimental $d\alpha/dT$ data when the number of reactions is increased, followed by the reaction scheme composed of consecutive reactions. As the parallel reaction scheme consists in adding independent reactions, and because the optimization is realized on 4 different parameters (E_i, A_i, n_i, X_i), the parallel reaction scheme is less constrained than the consecutive and competitive schemes. Therefore, the better agreement obtained with the parallel scheme could be the result of the lack of constraints on the scheme, and therefore the good quality of fit could be due to mathematical causes rather than physical considerations. R^2 roughly stagnates for competitive reactions, showing that adding this type of reactions does not improve the model agreement against experimental mass loss rates.

Figure 9 represents the residual mass as a function of heating rates for all the schemes.

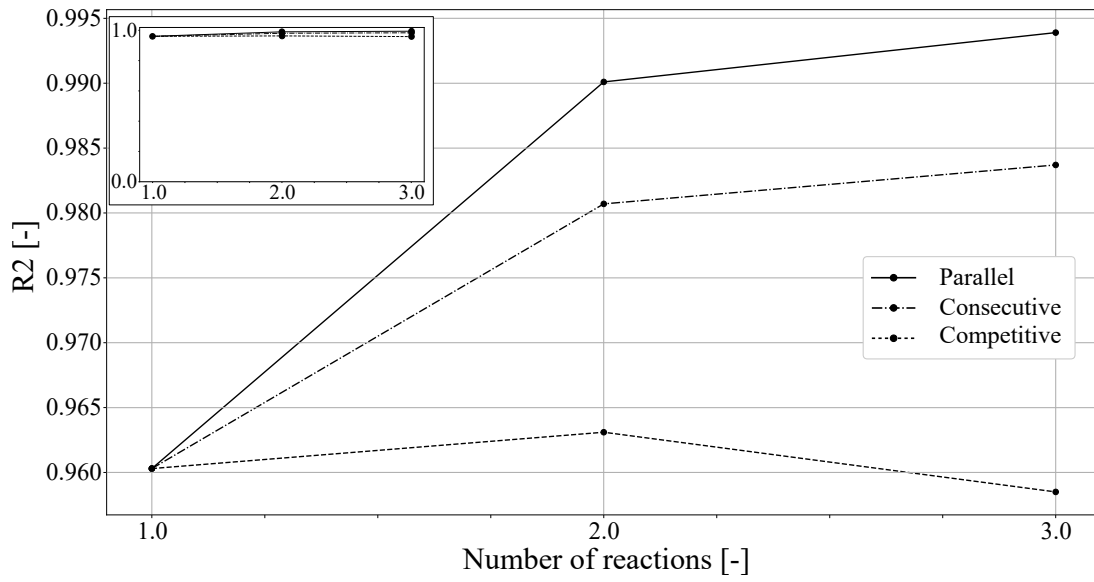


Figure 7: Evolution of the coefficient of determination (R^2) as a function of the number and nature of intermediate reactions used in the reaction scheme under an inert atmosphere.

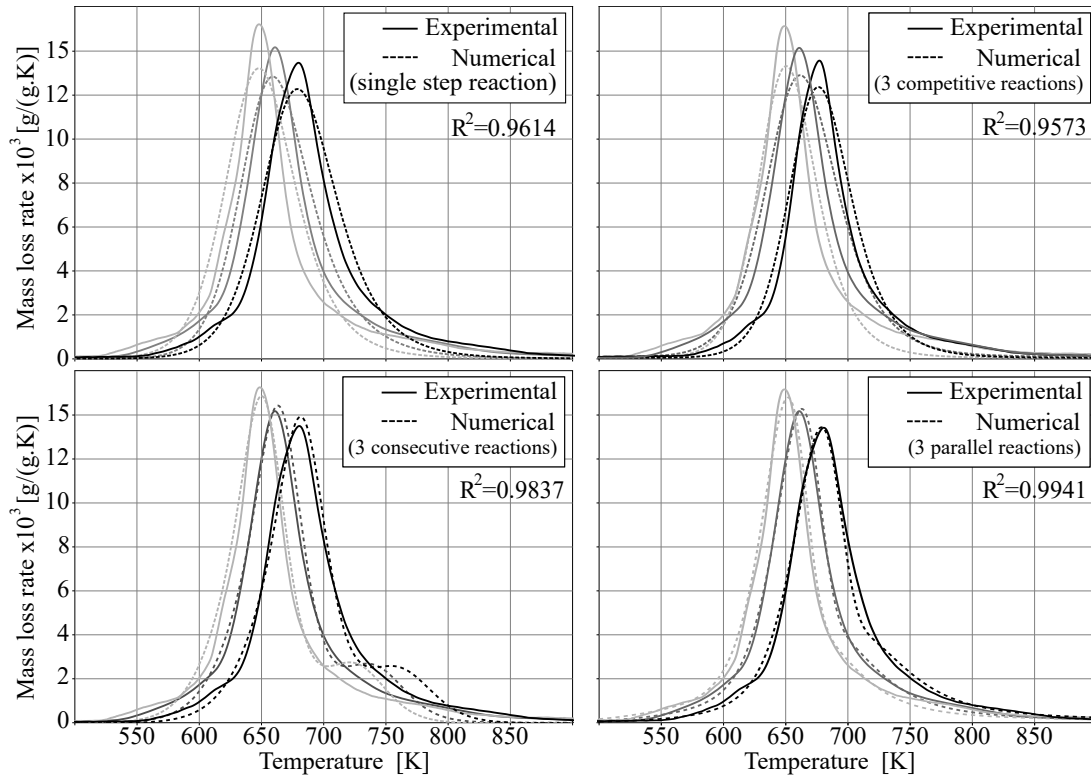


Figure 8: Comparison between mass loss rates from anaerobic TGA experiments and kinetic modeling for different reaction schemes. \square : $\beta = 5 \text{ K min}^{-1}$, \blacksquare : $\beta = 10 \text{ K min}^{-1}$, \blacksquare : $\beta = 25 \text{ K min}^{-1}$.

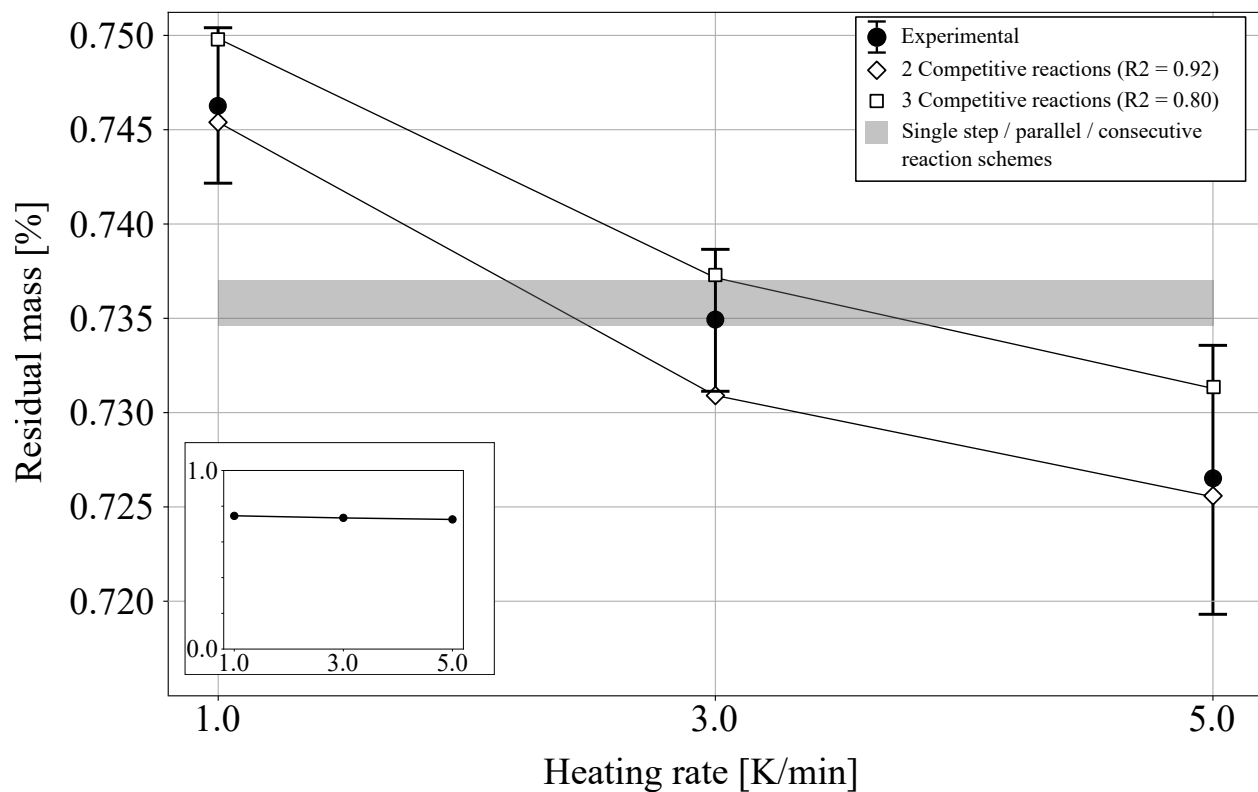


Figure 9: Evolution of the residual mass as a function of the heating rate for anaerobic pyrolysis of carbon/epoxy composite, comparing experimentally obtained values to the modeling results using different reaction schemes.

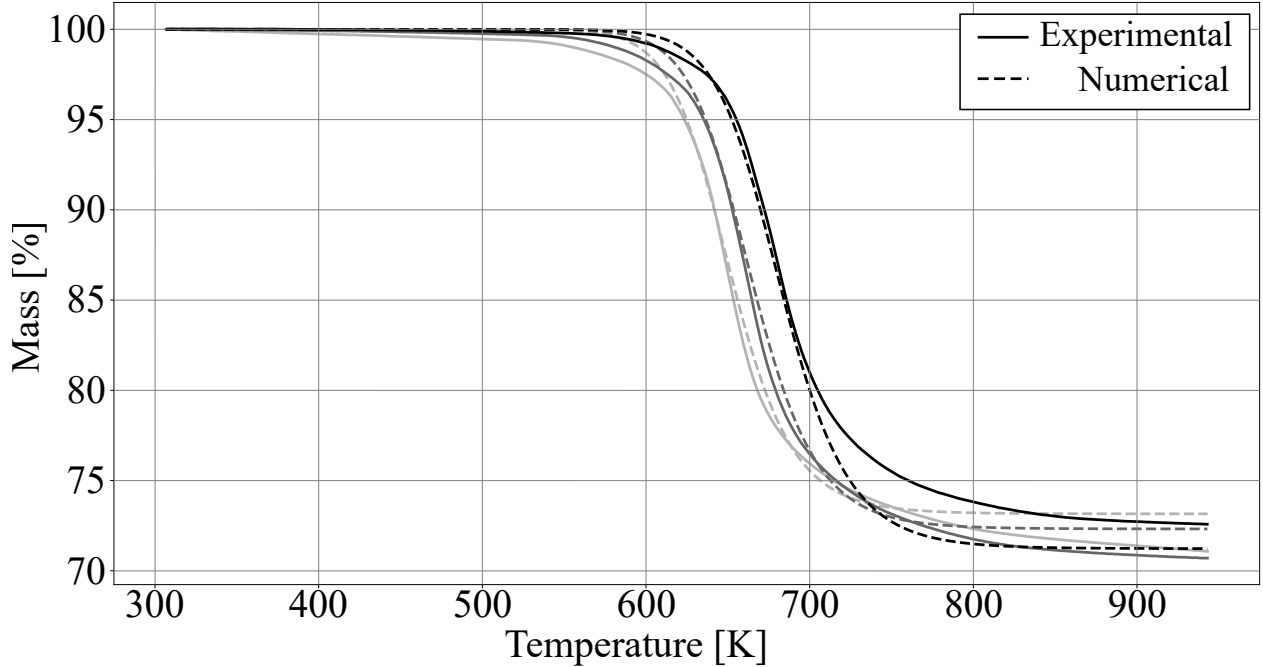


Figure 10: Variation of mass as a function of temperature under inert atmosphere. The dashed lines depict the numerical data obtained with the reaction scheme composed of 2 competitive reactions (Table 5) and the continuous lines represent the mass measured with TGA.. \square : $\beta = 5 \text{ K min}^{-1}$, \blacksquare : $\beta = 10 \text{ K min}^{-1}$, \blacksquare : $\beta = 25 \text{ K min}^{-1}$.

The coefficient of determination has been added on Figure 9 to ease the comparison of the curves. It shows that the reaction schemes composed of parallel and consecutive reactions all provide a constant residual mass when the heating rate is changed, and therefore cannot accurately model the variation of residual mass observed in the tube furnace, even if these two schemes offered very good agreement against mass loss rate data. The competitive reaction models are the only ones capable of properly modeling a variable residual mass. This can be explained because a different char yield is associated with each competitive reaction. In such a scheme, some reactions can be promoted to the detriment of other reactions for low or high heating rates. Therefore, the global char yield varies for each heating rate, as it tends to the value provided by the dominant reaction. To summarize, reaction schemes composed of competitive reactions do not capture mass loss rate data as well as those composed of consecutive or parallel reactions, but are the only one able to properly capture the variation of residual mass as a function of heating rate. Having three competitive reactions

| Type | N | X_i ($\text{m}^3 \text{m}^{-3}$) | E (kJ mol^{-1}) | A (s^{-1}) | n (-) | θ_i (-) | R^2 (-) |
|-------------|---|--------------------------------------|------------------------------|-------------------------|---------|-----------------------|-----------|
| Single-step | 1 | - | 199.17 | 5.26×10^{13} | 2.43 | 0.3687 | 0.9614 |
| Competitive | 2 | - | 80 | 1.71×10^3 | 1.37 | 0.44 | 0.9631 |
| | | - | 241 | 1.21×10^{17} | 2.45 | 0.30 | |
| | 3 | - | 153 | 2.47×10^9 | 1.89 | 0.62 | 0.9573 |
| | | - | 178 | 3.09×10^{11} | 2.20 | 0.53 | |
| | | - | 203 | 3.96×10^{13} | 2.17 | 3.9×10^{-9} | |
| Parallel | 2 | 0.67 | 120 | 7.46×10^6 | 2.79 | 0.55 | 0.9900 |
| | | 0.33 | 214 | 7.90×10^{14} | 1.16 | 8.92×10^{-8} | |
| | 3 | 0.48 | 73.4 | 3.24×10^3 | 4.79 | 0.734 | 0.9941 |
| | | 0.23 | 152 | 2.94×10^9 | 2.09 | 2.57×10^{-8} | |
| | | 0.29 | 215 | 9.36×10^{14} | 1.06 | 2.20×10^{-8} | |
| Consecutive | 2 | - | 185 | 2.13×10^{13} | 2.5 | 0.81 | 0.9807 |
| | | - | 200 | 1.49×10^{14} | 2.49 | 0.45 | |
| | 3 | - | 170 | 4.99×10^{11} | 1.5 | 0.79 | 0.9837 |
| | | - | 190 | 1.35×10^{13} | 1.5 | 0.61 | |
| | | - | 200 | 1.01×10^{12} | 1.5 | 0.77 | |

Table 5: Single-step and multi-step reaction schemes describing the pyrolysis of an epoxy resin exposed to an inert atmosphere for heating rates $\beta = 5, 10, 25 \text{ K min}^{-1}$. The residue (Equation 10) is calculated with $x = \alpha$ for all the schemes.

instead of two decreases simultaneously the agreement against experimental mass loss rate ($R^2 = 0.9573$ vs $R^2 = 0.9631$) and residual mass ($R^2 = 0.80$ vs $R^2 = 0.92$), showing that the optimum number of competitive reactions is two. Figure 10 shows the variation of mass as a function of time under inert atmosphere. The measurements obtained from TGA (continuous line) are compared to the outcomes obtained with the reaction scheme composed of two competitive reactions in Table 5 (dashed line). The residual mass obtained with the two-competitive scheme is in the same range than the one obtained in TGA, which shows that the model is able to provide a realistic value of the residual mass even beyond the heating rates of the tube furnace. Moreover, contrary to the TGA data, the residual mass obtained with the two-competitive scheme decreases monotonically with the heating rate, with a variation of 3% for $\beta = 5 - 25 \text{ K min}^{-1}$. This variation could be even more important in a fire test where $\beta > 500 \text{ K min}^{-1}$.

These results confirm the tendency observed in the literature that adding intermediate reactions can improve the agreement against mass loss rate data. However, it also shows that a reaction scheme can simultaneously capture the mass loss rate with a good quality of fit, but not the residual mass. In the literature, reaction schemes are typically chosen to maximize the agreement against mass loss rate data. In that case, the reaction scheme

composed of parallel reactions should be the best, as it provides the best coefficient of determination; however, this parallel reaction scheme is unable to model the variation of residual mass observed in the tube furnace. The char yield controls the quantity of protective char and combustible gases formed during the pyrolysis, and therefore influences the material thermal decomposition. In some cases, the reaction rate and char yield can have an almost comparable influence on the thermal response of a composite exposed to heat source [5]. The differences of residual mass observed in this study remain low in absolute terms for the composite as a whole, but are more significant relative to the char-forming fraction of the material (matrix). Moreover, these differences could rise with higher heating rates, or with different polymers. Consequently, optimizing a reaction scheme to obtain a best fit against experimental mass loss rate only, as usually done in the literature, could lead to inaccurate predictions if the reaction scheme is intended to be used in a composite pyrolysis model. However, a need remains to investigate the effect of optimizing the mass loss rate at the expense of the residual mass.

5. Conclusion

Pyrolysis models are widely used to predict the behavior of composites exposed to high temperatures. Due to the sensitivity of these predictive tools to the thermo-chemical decomposition of the resin, different reaction schemes of increasing complexity are implemented in the literature to best represent TGA data. A popular strategy consists in adding intermediate reactions of different nature (parallel, competitive, consecutive) to obtain the best fit with the experimental mass loss rate. However, the optimal number and nature of intermediate reactions is rarely discussed.

In this paper, the thermo-chemical parameters (E , A and n) describing the pyrolysis of an epoxy resin, as well as the oxidation of char and carbon fibers have been extracted from TGA data using isoconversional methods. Several reaction schemes of variable complexity are proposed and assessed. A first single-step scheme modeled the mass loss rate observed

in TGA with a very good agreement, but was unable to model the variation of residual mass observed in a tube furnace when the heating rate is changed. For this reason, several multi-steps schemes have been developed and compared, with an increasing number of reactions of different nature. Results show that even if the addition of parallel or consecutive reactions improves the agreement against TGA data, these schemes are unable to account for the variation of residual mass observed in a tube furnace. Although, adding competitive reactions does not improve the agreement with TGA data compared to a single-step scheme, only this type of reaction allows to model the variation of residual mass with a very good agreement. More research is needed to test reaction schemes including simultaneously competitive, consecutive and parallel intermediate reactions.

This research suggests that contrary to what is commonly done in the literature, obtaining a best fit between experimental and numerical TGA data is not sufficient to build a realistic reaction scheme. Considering the influence of the char yield in heat transfer processes, the residual mass should also be considered when developing a reaction scheme that is intended to be implemented in a pyrolysis model. The variation of residual mass of the carbon/epoxy composite studied here remains low but could be more important for other materials. Further research is needed to find the right balance between accurate modeling of E/A and accurate modeling of θ , if a good agreement cannot be obtained simultaneously on these two variables. This issue could be addressed by investigating the sensitivity of pyrolysis models to reaction schemes of different nature, for different classes of materials.

Conflict of interest statement

No conflict of interest needs to be reported.

Acknowledgments

We are grateful for the assistance and financial support from the Natural Sciences and Engineering Research Council of Canada (NSERC/CRSNG), through grant no. CRDPJ

478687-15, and the partners from CRIAQ ENV-708 project is acknowledged. One of the authors (PCG) is grateful to the National Science and Technology Council of Mexico (CONACYT) for his doctoral scholarship.

References

- [1] L. Nicolais, M. Meo, and E. Milella, *Composite materials: A Vision for the Future*. springer ed., 2011.
- [2] ISO2685:1998(E), “Aircraft - Environmental Test Procedure for Airborne Equipment - Resistance to Fire in Designated Fire Zones,” *the International Organization for Standardization (ISO): Geneva, Switzerland*, 1998.
- [3] A. Mouritz, S. Feih, E. Kandare, Z. Mathys, A. Gibson, P. Des Jardin, S. Case, and B. Y. Lattimer, “Review of fire structural modelling of polymer composites,” *Composites Part A: Applied Science and Manufacturing*, vol. 40, no. 12, pp. 1800–1814, 2009.
- [4] C. Lautenberger and A. Fernandez-Pello, “Generalized pyrolysis model for combustible solids,” *Fire Safety Journal*, vol. 44, no. 6, pp. 819–839, 2009.
- [5] S. I. Stoliarov and R. Lyon, “Thermo-kinetic model of burning for pyrolyzing materials,” *Fire Safety Science - Proceedings of the ninth international symposium*, pp. 1141–1152, 2008.
- [6] K. McGrattan, S. Hostikka, R. McDermott, J. Floyd, C. Weinschenk, and K. Overholt, “Fire Dynamics Simulator technical reference guide volume 2: Mathematical model,” tech. rep., NIST, 2016.
- [7] A. Snegirev, V. Talalov, V. Stepanov, and J. Harris, “A new model to predict pyrolysis, ignition and burning of flammable materials in fire tests,” *Fire Safety Journal*, vol. 59, pp. 132–150, 2013.
- [8] S. I. Stoliarov, N. Safronava, and R. Lyon, “The effect of variation in polymer properties on the rate of burning,” *Fire and Materials*, vol. 33, pp. 257–271, 2009.
- [9] M. Chaos, “Application of sensitivity analyses to condensed-phase pyrolysis modeling,” *Fire Safety Journal*, vol. 61, pp. 254–264, 2013.
- [10] J. C. Paterson-Jones, “The mechanism of the thermal degradation of aromatic amine-cured glycidyl ether-type epoxide resins,” *Journal of Applied Polymer Science*, vol. 19, no. 6, pp. 1539–1547, 1975.

- [11] K. S. Chen and R. Z. Yeh, "Pyrolysis kinetics of epoxy resin in a nitrogen atmosphere," *Journal of Hazardous Materials*, vol. 49, no. 2-3, pp. 105–113, 1996.
- [12] S. Montserrat, J. Málek, and P. Colomer, "Thermal degradation kinetics of epoxy–anhydride resins: I.," *Thermochimica Acta*, vol. 313, no. 1, pp. 83–95, 1998.
- [13] L. A. Burns, S. Feih, and A. Mouritz, "Fire-Under-Load Testing of Carbon Epoxy Composites," *Aerospace Engineering*, vol. 222, pp. 1–10, 2009.
- [14] C. Branca, C. Di Blasi, A. Galgano, and E. Milella, "Thermal and kinetic characterization of a toughened epoxy resin reinforced with carbon fibers," *Thermochimica Acta*, vol. 517, no. 1-2, pp. 53–62, 2011.
- [15] M. McGurn, P. E. Desjardin, and A. B. Dodd, "Numerical simulation of expansion and charring of carbon-epoxy laminates in fire environments," *International Journal of Heat and Mass Transfer*, vol. 55, no. 1-3, pp. 272–281, 2012.
- [16] R. D. Chippendale, I. O. Golosnoy, and P. L. Lewin, "Numerical modelling of thermal decomposition processes and associated damage in carbon fibre composites," *Journal of Physics D: Applied Physics*, vol. 47, no. 38, 2014.
- [17] P. Tadini, N. Grange, K. Chetehouna, N. Gascoin, S. Senave, and I. Reynaud, "Thermal degradation analysis of innovative PEKK-based carbon composites for high-temperature aeronautical components," *Aerospace Science and Technology*, vol. 65, pp. 106–116, 2017.
- [18] S. Vyazovkin, A. K. Burnham, J. M. Criado, L. A. Pérez-Maqueda, C. Popescu, and N. Sbirrazzuoli, "ICTAC Kinetics Committee recommendations for performing kinetic computations on thermal analysis data," *Thermochimica Acta*, vol. 520, no. 1-2, pp. 1–19, 2011.
- [19] G. Rein, C. Lautenberger, A. C. Fernandez-Pello, J. L. Torero, and D. L. Urban, "Application of genetic algorithms and thermogravimetry to determine the kinetics of polyurethane foam in smoldering combustion," *Combustion and Flame*, vol. 146, no. 1-2, pp. 95–108, 2006.
- [20] E. Kim, N. Dembsey, and S. Shivkumar, "Evaluating effects of applying different kinetic models to pyrolysis modeling of fiberglass-reinforced polymer composites," *Fire and Materials*, vol. 39, pp. 153–173, 2015.
- [21] M. Mckinnon, Y. Ding, S. I. Stoliarov, S. Crowley, and R. E. Lyon, "Pyrolysis model for a carbon fiber/epoxy structural aerospace composite," *Journal of Fire Sciences*, vol. 1, 2016.

- [22] P. Tranchard, S. Duquesne, F. Samyn, B. Estèbe, and S. Bourbigot, “Kinetic analysis of the thermal decomposition of a carbon fibre-reinforced epoxy resin laminate,” *Journal of Analytical and Applied Pyrolysis*, vol. 126, no. May, pp. 14–21, 2017.
- [23] E. Moukhina, “Determination of kinetic mechanisms for reactions measured with thermoanalytical instruments,” *Journal of Thermal Analysis and Calorimetry*, vol. 109, no. 3, pp. 1203–1214, 2012.
- [24] C. Lautenberger and C. Fernandez-pello, “A model for the oxidative pyrolysis of wood,” *Combustion and Flame*, vol. 156, no. 8, pp. 1503–1513, 2009.
- [25] M. Olave, A. Vanaerschot, S. Lomov, and D. Vandepitte, “Internal Geometry Variability of Two Woven Composites and Related Variability of the Stiffness,” *Polymer Composites*, vol. 33, pp. 1335–1350, 2012.
- [26] F. Gommer, A. Endruweit, and A. C. Long, “Quantification of micro-scale variability in fibre bundles,” *Composites Part A: Applied Science and Manufacturing*, vol. 87, pp. 131–137, 2016.
- [27] S. S. Park, D. K. Seo, S. H. Lee, T. U. Yu, and J. Hwang, “Study on pyrolysis characteristics of refuse plastic fuel using lab-scale tube furnace and thermogravimetric analysis reactor,” *Journal of Analytical and Applied Pyrolysis*, vol. 97, pp. 29–38, 2012.
- [28] K. Le Manquais, C. Snape, J. Barker, and I. McRobbie, “TGA and drop tube furnace investigation of alkali and alkaline earth metal compounds as coal combustion additives,” *Energy and Fuels*, vol. 26, no. 3, pp. 1531–1539, 2012.
- [29] J. Zsakó, “Remarks on ”A new equation for modelling nonisothermal reactions”,” *Journal of Thermal Analysis*, vol. 34, no. 5-6, pp. 1489–1494, 1988.
- [30] M. J. Starink, “The determination of activation energy from linear heating rate experiments: A comparison of the accuracy of isoconversion methods,” *Thermochimica Acta*, vol. 404, no. 1-2, pp. 163–176, 2003.
- [31] H. E. Kissinger, “Variation of peak temperature with heating rate in differential thermal analysis,” *Journal of Research of the National Bureau of Standards*, vol. 57, no. 4, p. 217, 1956.
- [32] T. Ozawa, “A New Method of Analyzing Thermogravimetric Data,” *Bulletin of the Chemical Society of Japan*, vol. 38, no. 11, pp. 1881–1886, 1965.
- [33] J. Flynn and L. Wall, “A quick, direct method for the determination of activation energy from thermogravimetric data,” *Polymer letters*, vol. 322, no. 1211, pp. 379–400, 1966.

- [34] R. Lyon, “An integral method of non-isothermal kinetic analysis,” tech. rep., Federal Aviation Administration, 1996.
- [35] J. H. Flynn, “The ”temperature integral” - Its use and abuse,” *Thermochimica Acta*, vol. 300, no. 1-2, pp. 83–92, 1997.
- [36] J. A. Quintiere, R. N. Walters, and S. Crowley, “Flammability Properties of Aircraft Carbon-Fiber Structural Composite,” Tech. Rep. October, Federal Aviation Administration, 2007.
- [37] N. Sbirrazzuoli, “Determination of pre-exponential factors and of the mathematical functions $f(\alpha)$ or $G(\alpha)$ that describe the reaction mechanism in a model-free way,” *Thermochimica Acta*, vol. 564, pp. 59–69, 2013.
- [38] R. Iacocca and D. Duquette, “The catalytic effect of platinum on the oxidation of carbon fibres,” *Journal of Materials Science*, vol. 28, pp. 1113–1119, 1993.
- [39] V. Biasi, *Modelisation Thermique de la Dégradation d’un Matériau Composite Soumis au Feu*. Thèse de doctorat, Université de Toulouse, 2014.
- [40] A. Adumitroaie and E. J. Barbero, “Beyond plain weave fabrics - II. Mechanical properties,” *Composite Structures*, vol. 93, no. 5, pp. 1449–1462, 2011.
- [41] S. Vyazovkin, K. Chrissafis, M. L. Di Lorenzo, N. Koga, M. Pijolat, B. Roduit, N. Sbirrazzuoli, and J. J. Suñol, “ICTAC Kinetics Committee recommendations for collecting experimental thermal analysis data for kinetic computations,” *Thermochimica Acta*, vol. 590, pp. 1–23, 2014.
- [42] A. De Fenzo, C. Formicola, V. Antonucci, M. Zarrelli, and M. Giordano, “Effects of zinc-based flame retardants on the degradation behaviour of an aerospace epoxy matrix,” *Polymer Degradation and Stability*, vol. 94, no. 9, pp. 1354–1363, 2009.
- [43] N. Rose, M. Le Bras, S. Bourbigot, R. Delobel, and B. Costes, “Comprehensive study of the oxidative degradation of an epoxy resin using the degradation front model,” *Polymer Degradation and Stability*, vol. 54, no. 2-3, pp. 355–360, 2002.
- [44] “Carbon Fiber Production using a PAN Precursor,” in *Carbon Fibers and their Composites* (P. Morgan, ed.), Taylor & Francis, 2005.
- [45] M. K. Ismail, “On the reactivity, structure, and porosity of carbon fibers and fabrics,” *Carbon*, vol. 29, no. 6, pp. 777–792, 1991.

- [46] M. C. Halbig, J. D. McGuffin-Cawley, A. J. Eckel, and D. N. Brewer, “Oxidation Kinetics and Stress Effects for the Oxidation of Continuous Carbon Fibers within a Microcracked C/SiC Ceramic Matrix Composite,” *Journal of the American Ceramic Society*, vol. 91, no. 2, pp. 519–526, 2008.
- [47] M. Newville and T. Stensitzki, “Non-Linear Least-Squares Minimization and Curve-Fitting for Python,” 2018.